



Crystal and magnetic structures of the Ir(V) $J_{\text{eff}}^{\text{Ir}} = 0$ double perovskite LaSrNiIrO_6

Xabier Martínez de Irujo-Labalde, Jacob E. Page, Harry W.T. Morgan, John E. McGrady, Michael A. Hayward*

Department of Chemistry, University of Oxford, Inorganic Chemistry Laboratory, South Parks Road, Oxford, OX1 3QR, UK

ARTICLE INFO

Keywords:

3d-5d double Perovskite
Magnetic structure
Neutron diffraction
DFT

ABSTRACT

LaSrNiIrO_6 adopts a B-site cation-ordered double perovskite structure with a strong $a^-a^-c^+$ cooperative tilting distortion (space group $P2_1/n$ $a = 5.5931(1) \text{ \AA}$, $b = 5.5676(1) \text{ \AA}$, $c = 7.8850(1) \text{ \AA}$, $\beta = 90.01(1)^\circ$). Magnetization and neutron diffraction data indicate LaSrNiIrO_6 adopts a 'type II' antiferromagnetic structure ($T_N = 70 \text{ K}$) in which the Ni spins are arranged in an antiferromagnetic manner with their next-nearest-neighbors, with no ordered moment observed for Ir. DFT calculations, including spin-orbit coupling effects, confirm $S = 1 \text{ Ni}^{2+}$ and $J_{\text{eff}} = 0 \text{ Ir}^{5+}$ local configurations and indicate strong $\text{Ni}(3d_{x^2-y^2})^1 - \text{O}(2p) - \text{Ir}(5d_{x^2-y^2})^0 - \text{O}(2p) - \text{Ni}(3d_{x^2-y^2})^1$ σ -type super-super-exchange is the dominant magnetic coupling interaction in the system.

1. Introduction

Complex transition-metal oxides containing both 3d and 5d transition metal cations have attracted considerable attention as their physical behavior is often complex and not easily explained as a simple combination of component parts [1]. For example, perovskite oxides which only contain 3d transition metals tend to be insulating (narrow 3d bands, large onsite repulsion, U) with metal cations adopting high-spin states (modest crystal field, Δ). The dominant magnetic interactions in these insulating phases are super exchange couplings, which are generally well described using the Goodenough-Kanamori rules [2]. In contrast the complex oxides of 5d metals are more likely to be metallic (wide 5d bands, small U) and tend to adopt low-spin states (large Δ) with local electronic configurations which are further complicated by strong spin orbit coupling (SOC) [3,4].

Systems which contain both 3d and 5d transition metals, such as $\text{A}_2\text{BB}'\text{O}_6$ double perovskite oxides, can show a wide variety of ordered magnetic states which cannot be easily understood on the basis of simple nearest-neighbor coupling interactions [1,5–7]. One such family of materials are the double perovskite oxides containing ordered arrays of Ir^{5+} and a 3d transition metal cation (Fe^{3+} , Co^{3+} , Co^{2+} , Ni^{2+} , Cu^{2+}) which exhibit 'type II' antiferromagnetic ground states which do not appear to be the result of nearest neighbor super exchange coupling [8–15]. This magnetic ordering scheme contrasts with the 'type I' arrangement observed for the isovalent phase LaSrNiSbO_6 in which $d^{10} \text{ Sb}^{5+}$ replaces

the Ir^{5+} in the extended oxide lattice [16].

The nature of the magnetic ordering in $\text{A}_2\text{B}^{\text{Ir}^{5+}}\text{O}_6$ double perovskite oxides can be attributed to the unusual local electronic state adopted by iridium in these phases. When octahedrally coordinated, $d^4 \text{ Ir}^{5+}$ adopts a diamagnetic electronic configuration for which there is no analogue among 3d transition metal cations. This $J_{\text{eff}} = 0$ configuration arises from the simultaneous application of a strong crystal field, which splits the iridium 5d orbitals into the familiar t_{2g} and e_g sets, and strong SOC which further splits the t_{2g} orbitals into quartet $J = 3/2$ and doublet $J = 1/2$ states. The energy gap between the $J = 3/2$ and $J = 1/2$ states is large, with the $J = 3/2$ state lying at lower energy, so the d^4 electron count of Ir^{5+} completely fills the $J = 3/2$ level, resulting in a diamagnetic configuration [17].

When arranged in $\text{A}_2\text{M}^{\text{Ir}^{5+}}\text{O}_6$ ($\text{M} = 3d$ transition metal) double perovskite oxide phases, the diamagnetic configuration of Ir^{5+} means that the accompanying 3d transition metal centers are widely separated ($\text{M}-\text{M} \sim 5.5 \text{ \AA}$) within a diamagnetic framework, yet these systems exhibit long-range magnetic order, to temperatures exceeding 100 K in the case of $\text{Sr}_2\text{FeIrO}_6$ [8,9]. This suggests that strong magnetic exchange pathways exist in these phases, and given the arrangement of the metal cations, these pathways are likely to involve the Ir centers in some capacity, as has been observed in other 3d-5d double perovskite oxide systems [7].

A previous report indicated LaSrNiIrO_6 adopts an $a^-a^-c^+$ distorted, B-cation ordered double perovskite structure, as determined by powder X-

* Corresponding author.

E-mail address: michael.hayward@chem.ox.ac.uk (M.A. Hayward).

<https://doi.org/10.1016/j.jssc.2022.123477>

Received 1 July 2022; Received in revised form 1 August 2022; Accepted 3 August 2022

Available online 18 August 2022

0022-4596/© 2022 The Authors. Published by Elsevier Inc. This is an open access article under the CC BY license (<http://creativecommons.org/licenses/by/4.0/>).

ray diffraction, with magnetization data suggesting a low-temperature antiferromagnetic state [14]. Here we describe a study using neutron diffraction data which not only allows accurate M – O bond lengths to be determined, but crucially enables the nature of the low-temperature magnetic state to be determined, allowing the role of Ir⁵⁺ in the magnetic coupling interactions in this material to be investigated via computation.

2. Experimental section

Sample preparation. A sample of LaSrNiIrO₆ was prepared using a citrate gel method. Appropriate quantities of SrCO₃ (99.994%), La₂O₃ (99.99%, dried at 900 °C) and Ni (99.996%) were dissolved in a minimal quantity of a 1:1 mixture of conc. nitric acid and distilled water, then the required amount of IrO₂ (99.99%, dried at 700 °C for 2 h) was added. Citric acid and analar ethylene glycol were added, and the solution was heated whilst being stirred. The gel thus formed was allowed to combust in air and the subsequent product was ground into a fine powder, placed in an alumina crucible and heated at 1000 °C in air at a rate of 1 °C min⁻¹ to remove the organic components of the sample. The resulting powder was pressed into a 13 mm diameter pellet and heated in air for 2 days at 1200 °C and 2 days at 1300 °C.

Characterization. X-ray powder diffraction data were collected from using instrument I11 at the Diamond Light Source Ltd. Samples were ground with amorphous boron to limit X-ray absorption and minimize preferred orientation and were sealed inside 0.5 mm diameter borosilicate glass capillaries. Diffraction patterns were measured using Si-calibrated X-rays with an approximate wavelength 0.825 Å using the PSD detector. Neutron powder diffraction data were collected at a wavelength of 1.5943 Å using the D2B instrument, at the ILL neutron source, from samples contained within vanadium cans. Rietveld profile refinements were performed using the TOPAS suite of programs (v6) [18]. Magnetization data were collected using a Quantum Design MPMS SQUID magnetometer.

Computational methods. All density functional theory calculations were carried out using the VASP software package [19,20], version 5.3.5, with the PBE functional [21] and a plane-wave cutoff of 600 eV. The effect of the core electrons was incorporated using PAW potentials [22], and Hubbard *U*_{eff} values of 6.0 eV and 2.0 eV were used for Ni and Ir, respectively [23]. For the *J*- and *D*-type unit cells, the Brillouin zone was sampled on 3 × 6 × 2 and 4 × 4 × 2 Γ -centered grids, respectively [24]. Spin-orbit coupling is included [25] with quantization axis along (0,0,1).

3. Results and discussion

Structural characterization. Synchrotron X-ray and neutron powder diffraction data collected from LaSrNiIrO₆ at room temperature could be readily indexed using a monoclinic unit cell *a* = 5.593 Å, *b* = 5.567 Å, *c* = 7.885 Å, β = 90.01° and extinction conditions consistent with P2₁/*n* space group symmetry. These parameters suggest a B-cation ordered perovskite structure with an *a*⁻*a*⁺*c*⁺ tilting distortion, consistent with previous reports on LaSrNiIrO₆ and analogous to the structure reported for LaSrCoIrO₆ [12,14]. Therefore a model based on the reported structure of LaSrNiIrO₆ was constructed and refined simultaneously against both the X-ray and neutron diffraction data. A combined X-ray/neutron data refinement as required to accurately study the Ni/Ir order of the phase as these elements have very similar neutron scattering lengths (Ni = 10.3 fm, Ir = 10.6 fm) [26]. The refinement converged smoothly to give a good statistical fit to both data sets. Full details of the refined structure of LaSrNiIrO₆ are given in Table 1, with selected bond lengths and angles in Table 2. Plots of observed and calculated data are shown in Fig. 1, and a representation of the structure is shown in Fig. 2.

The refined structure detailed in Table 1 is broadly in line with the structure determined previously from X-ray powder diffraction data [14], differing only in the details of the oxide ion locations, as expected. The bond lengths determined for the Ni^{II}O₆ and Ir^VO₆ units (Table 2) yield

Table 1

Structural parameters for LaSrNiIrO₆ from the simultaneous refinement against neutron and X-ray powder diffraction data collected at 298K.

	x	y	z	Fraction	B _{iso} (Å ²)
La/Sr	0.9964(6)	0.0266(3)	0.2513(6)	0.5/0.5	0.32(1)
Ni(1)/ Ir(1)	½	0	½	0.984(1)/ 0.016(1)	0.05(1)
Ir(2)/ Ni(2)	½	0	0	0.984(1)/ 0.016(1)	0.05(1)
O(1)	0.0673(8)	0.4918(6)	0.2514(31)	1	0.51(4)
O(2)	0.7120(15)	0.2822(22)	0.0305(10)	1	0.76(3)
O(3)	0.2276(15)	0.2227(23)	0.9618(10)	1	0.66(2)
LaSrNiIrO ₆ – Space Group: P2 ₁ / <i>n</i> (#14)					
<i>a</i> = 5.5931(1) Å, <i>b</i> = 5.5676(1) Å, <i>c</i> = 7.8850(1) Å, β = 90.01(1)°					
volume = 245.54(1) Å ³					
Formula weight = 573.44 g mol ⁻¹ , Z = 2					
Radiation source: Synchrotron X-ray, λ = 0.8268 Å; neutron λ = 1.5943 Å					
Temperature: 298 K					
<i>R</i> _p = 1.38%, <i>wR</i> _p = 2.38%, SXR <i>R</i> _{Bragg} = 1.01%, NPD <i>R</i> _{Bragg} = 1.94					

Table 2

Selected bond lengths and angles from the structural refinement of LaSrNiIrO₆ at 298 K and 5K.

Cation	Anion	Bond Length 298 K (Å)	Bond Length at 5K (Å)
Ni(1)/Ir(1)	O(1)	2.018(24)	2.005(26)
	O(2)	2.031(10)	2.038(11)
	O(3)	2.024(11)	2.019(12)
Ir(2)/Ni(2)	O(1)	1.997(24)	2.007(26)
	O(2)	1.983(11)	1.983(12)
	O(3)	1.987(11)	1.982(11)
		Bond angle at 298 K (°)	Bond angle at 5 K (°)
Ni(1)-O(1)-Ir(2)		158.2(13)	157.7(14)
Ni(1)-O(2)-Ir(2)		158.9(5)	156.9(5)
Ni(1)-O(3)-Ir(2)		159.3(5)	159.9(5)

bond valence sums [27,28] of Ni+2.20 and Ir+4.92 respectively. The Ir–O bond lengths observed for LaSrNiIrO₆ are broadly in line with the values observed for Ir^{IV}O₆ units in other A₂Mir^{VI}O₆ double perovskite phases [8,10,12,13,15,29], with the IrO₆ unit being highly symmetric (close to O_h point group symmetry) in common with many other Ir^VO₆ units previously reported [8,9].

Magnetic characterization. Zero-field cooled and field-cooled magnetization data collected from LaSrNiIrO₆ as a function of temperature (Fig. 3) can be fitted by the Curie-Weiss law (χ = C/(T- θ)) in the temperature range 140 < T/K < 300 to yield values of C = 1.868(3) cm³ K mol⁻¹ and θ = -184.9(5) K, which is significantly larger than would be expected for a simple combination of S = 1, Ni²⁺ and J_{eff} = 0, Ir⁵⁺ (C_{expected} = 1 cm³ K mol⁻¹), as noted previously [14].

The magnetization data exhibit a maximum at T ~ 70 K consistent with the onset of magnetic order. Neutron powder diffraction data collected from LaSrNiIrO₆ at 5 K exhibit additional peaks compared to the analogous data collected at room temperature. These additional diffraction features can be indexed on the basis of a 1 × 2 × 2 geometric expansion of the crystallographic unit cell. A magnetic analysis using the ISODISTORT suite of programs [30,31] yielded two irreducible representations described in space groups 2.7 and 14.80 respectively, which both describe a type II antiferromagnetic structure and only differ in the orientation of the ordered moments (parallel to the x-axis or y-axis). Refinement of these models against the NPD data collected at 5 K revealed that the model described in magnetic space group 2.7, with ordered moments aligned parallel to the y-axis gave the best fit, yielding an ordered moment of 1.24 μ_B per Ni center and no detectable moment on the iridium centers. A complete description of the refined nuclear and magnetic models is given in Table 3 with selected bond lengths in Table 2 and a plot of the data in Fig. 4. A representation of the magnetic structure is shown in Fig. 2, with the monoclinic magnetic unit cell marked in red.

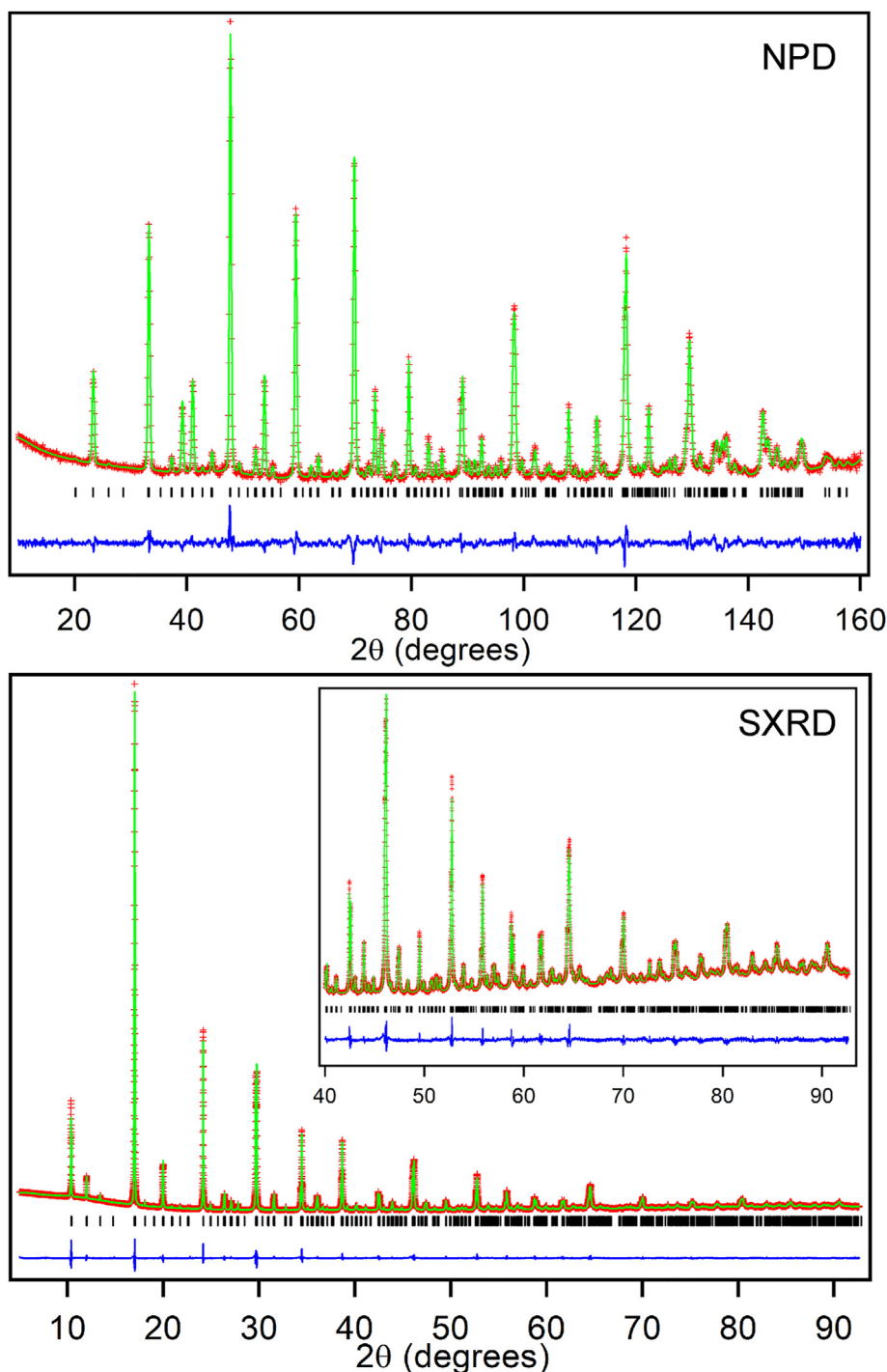


Fig. 1. Observed, calculated and difference plots for the simultaneous structural refinement of LaSrNiIrO₆ against NPD (top) and SXRD (bottom) data.

Electronic structure analysis. Our initial exploration of the electronic structure was based on spin-unrestricted DFT calculations using the unit cell shown in Fig. 5a, denoted the *J*-cell, which corresponds to the crystallographic unit cell described above, doubled along *a* and *c*. Relaxation of the lattice parameters gave optimized values of *a* = 11.25 Å, *b* = 5.67 Å and *c* = 15.87 Å, compared to experimental values of 11.186 Å, 5.567 Å and 15.770 Å. In the absence of spin-orbit coupling, the moments on the Ir and Ni centers are 1.75 μ_B and 1.14 μ_B, respectively, consistent with the local triplet configurations of both ions, modified by the greater covalence of the Ir–O bonds compared to Ni–O. The inclusion of spin-orbit coupling leaves the moment on Ni unchanged

but reduces that on Ir to 0.50 μ_B due to the population of the $J = 3/2$ spin-orbital coupled state of Ir⁵⁺ (*d*⁴). In the following discussion of magnetic coupling, we treat the Ir as effectively diamagnetic, as indicated by the magnetic measurements.

The DFT-computed energies are then mapped on to the diagonal elements of the Heisenberg spin Hamiltonian with *S*_{Ni} = 1, where the summation runs over only the paramagnetic Ni centers:

$$\hat{H}_{\text{HDVV}} = -\sum_{i,j} J_{ij} \hat{S}_i \cdot \hat{S}_j$$

Our approach to constructing a suitable spin Hamiltonian is to identify a minimal set of parameters that will yield an acceptable fit to the DFT energies. We initially chose a 4-parameter

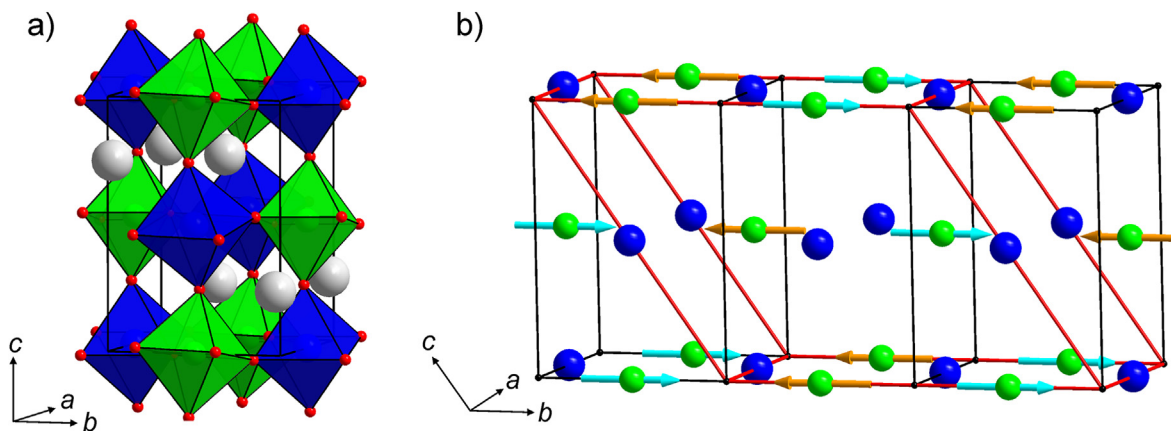


Fig. 2. a) The crystal structure of LaSrNiIrO_6 . b) The magnetic structure of LaSrNiIrO_6 . The crystallographic unit cell is marked in black, the magnetic unit cell is marked in red. Grey, green, blue and red spheres represent La/Sr, Ni, Ir and O respectively and orange and blue arrows indicate spin orientations.

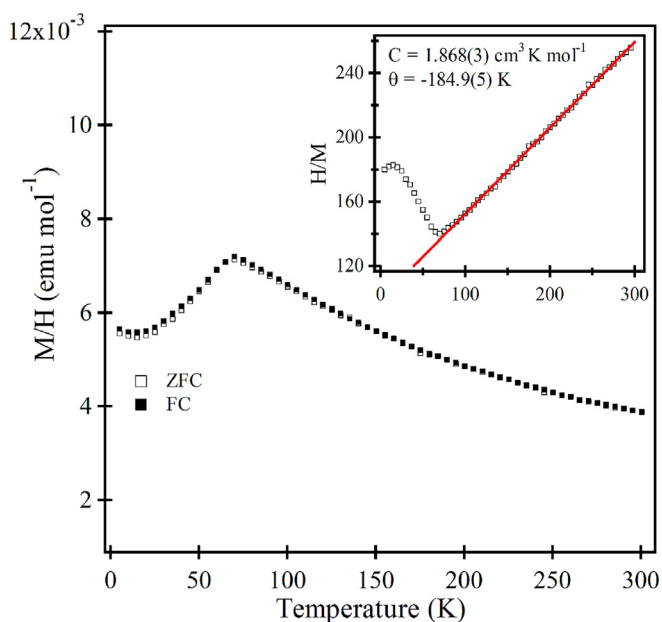


Fig. 3. Zero-field cooled and field cooled magnetization data collected from LaSrNiIrO_6 in an applied field of 100 Oe. Inset shows fit to Curie-Weiss law in the temperature range $140 < T/\text{K} < 300$.

Hamiltonian which includes the nearest-neighbor (NN) (J_1 and J_2), and next-nearest neighbor (NNN) (J_3 and J_4) Ni–Ni exchange couplings (see Fig. 5a and supporting information for full details of the calculations). The best fit set of parameters is: $J_1 = -1.8 \text{ cm}^{-1}$, $J_2 = -0.4 \text{ cm}^{-1}$, $J_3 = -17.8 \text{ cm}^{-1}$ and $J_4 = -11.4 \text{ cm}^{-1}$. From this analysis it is clear that the dominant contributions to the magnetic order come from the NNN Ni–Ni couplings (J_3 , J_4), both of which are antiferromagnetic, and much larger than their NN counterparts. Strong NNN coupling (“super-super-exchange”) is a well-established paradigm in double perovskites and related systems [32–34], and in this case the highly covalent nature of the $\text{Ir}^{\text{V}}\text{--O}$ bonds is clearly significant in mediating the strong $\text{Ni}(3d_{x^2-y^2})^1\text{--O}(2p)\text{--Ir}(5d_{x^2-y^2})^0\text{--O}(2p)\text{--Ni}(3d_{x^2-y^2})^1$ interactions that define J_3 and J_4 . Significant NNN couplings along M–O–M’–O–M chains have been noted to play a significant role in the magnetism of related perovskite systems [7,35].

The very marked $a^-a^+c^+$ tilting distortion in this system, resulting in Ir–O–Ni bond angles of 155° , complicates the analysis of the magnetic coupling pathway because the reduction in local symmetry at the metal

Table 3

Parameters for LaSrNiIrO_6 from nuclear and magnetic refinement against neutron powder diffraction data collected at 5 K.

	x	y	z	Fraction	$B_{\text{iso}} (\text{\AA}^2)$
La/Sr	0.9968(6)	0.0296(3)	0.2515(22)	0.5/0.5	0.16(1)
Ni(1)/Ir(1)	$\frac{1}{2}$	0	$\frac{1}{2}$	0.984/0.016	0.04(1)
Ir(2)/Ni(2)	$\frac{1}{2}$	0	0	0.984/0.016	0.04(1)
O(1)	0.0690(6)	0.4925(5)	0.2499(33)	1	0.29(1)
O(2)	0.7098(16)	0.2833(23)	0.0355(15)	1	0.32(2)
O(3)	0.2253(16)	0.2204(24)	0.9650(17)	1	0.31(2)
LaSrNiIrO_6 – Space Group: $P2_1/n$ (#14) $a = 5.5815(1) \text{ \AA}$, $b = 5.5633(1) \text{ \AA}$, $c = 7.8736(1) \text{ \AA}$, $\beta = 90.00(1)^\circ$ volume = $244.49(1) \text{ \AA}^3$ Formula weight = $573.44 \text{ g mol}^{-1}$, $Z = 2$ Magnetic space group: 2.7 , $a = 5.5815(1) \text{ \AA}$, $b = 9.6407(1) \text{ \AA}$, $c = 11.252(1) \text{ \AA}$, $\alpha = 125.2(1)^\circ$					
Ni	$\frac{1}{2}$	0	$\frac{1}{2}$	0.984	0.04(1)
$M_x (\mu_B)$		$M_y (\mu_B)$	$M_z (\mu_B)$		
	0	1.24(5)	0		
Radiation source: neutron $\lambda = 1.5943 \text{ \AA}$ Temperature: 5 K $R_p = 3.32\%$, $wR_p = 4.31\%$, $R_{\text{Bragg}} = 1.40$					

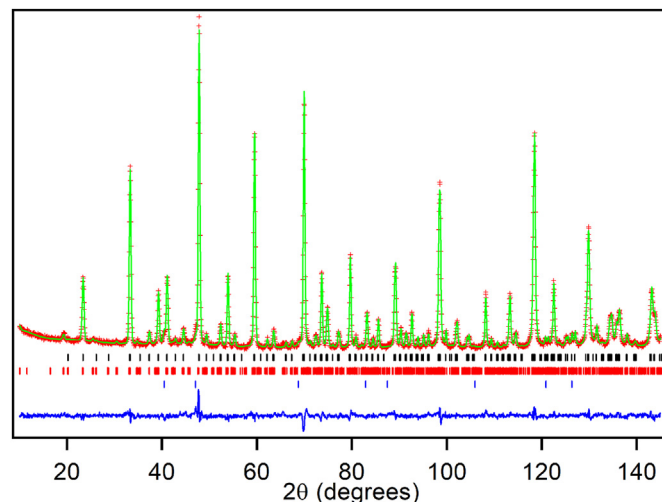


Fig. 4. Observed calculated and difference plots from the nuclear and magnetic structural refinement of LaSrNiIrO_6 against neutron powder diffraction data collected at 5 K. Top tick marks indicate nuclear peak positions, middle tick marks magnetic peak positions, bottom tick marks indicate contributions from sample environment.

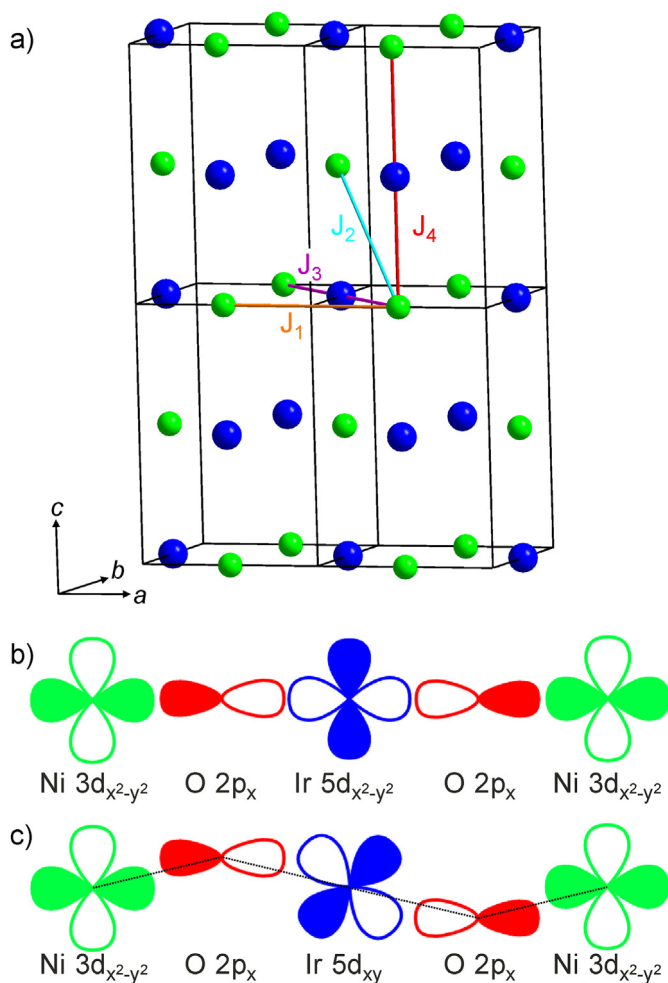


Fig. 5. a) Expanded 'J-cell' used in DFT calculations. Green and blue spheres represent Ni and Ir respectively. b) and c) Ni–O–Ir–O–Ni super-super-exchange pathways utilizing Ir 5d orbitals with σ and π symmetry respectively.

centers mixes the M – O π (t_{2g}) and M – O σ (e_g) pathways (Fig. 5b and c). It is possible, therefore, to envisage contributions to the NNN coupling from both pathways. In order to clarify this issue we have considered two further computational models, one where the $I4/m$ space group is imposed, enforcing linearity of the Ni–O–Ir triads along the c axis, and a second with $Fm\bar{3}m$ symmetry, where a perfect cubic arrangement with *all* bond angles at 180° is imposed. In the $I4/m$ model the coupling along the c axis (J_4) increases substantially in magnitude, to -55.9 cm^{-1} , while changes in the in-plane coupling (J_3) are much smaller. A further increase in symmetry to $Fm\bar{3}m$ causes only a modest further change in J_4 , but J_3 increases in magnitude to -58.9 cm^{-1} . The dramatic increase in the strength of the NNN couplings as linearity of the Ni–O–Ir bonds is imposed supports a model where the σ symmetry orbitals play a dominant role in the exchange coupling.

4. Conclusion

LaSrNiIrO₆ adopts a double perovskite structure in which Ni²⁺ and Ir⁵⁺ are ordered in an 'rock salt' manner. NPD data indicate that LaSrNiIrO₆ adopts a type II antiferromagnetic state below $T_N = 70 \text{ K}$ with an ordered moment of $1.24 \mu_B$ on each Ni site, and no observed moment of the Ir sites. DFT calculations show that strong spin orbit coupling reduces the local moment on the Ir⁵⁺ centers so they are effectively diamagnetic ($J_{\text{eff}} = 0$). Furthermore, calculations indicate that the dominant magnetic coupling interaction is a Ni($3d_{x^2-y^2}$)¹–O($2p$)–Ir($5d_{x^2-y^2}$)⁰–O($2p$)–Ni($3d_{x^2-y^2}$)¹ exchange which is observed to strengthen as the Ni–O–Ir

bond angles tend to 180° , consistent with a σ -type exchange pathway.

CRedit authorship contribution statement

Xabier Martínez de Irujo-Labalde: Data curation. Jacob E. Page: Data curation. Harry W.T. Morgan: Formal analysis.

Declaration of competing interest

The authors declare that they have no known competing financial interests or personal relationships that could have appeared to influence the work reported in this paper.

Data availability

Data will be made available on request.

Acknowledgements

We thank The Leverhulme Trust grant award RPG-2014-366 "Topochemical reduction of 4d and 5d transition metal oxides" for supporting this work. Experiments at the Diamond Light Source were performed as part of the Block Allocation Group award "Oxford Solid State Chemistry BAG to probe composition-structure-property relationships in solids" (CY25166). We thank E. Suard for assistance in collecting the NPD data. H.W.T.M. thanks the EPSRC for support through the Centre for Doctoral Training, Theory and Modelling in Chemical Sciences under Grant EP/L015722/1.

Appendix A. Supplementary data

Supplementary data to this article can be found online at <https://doi.org/10.1016/j.jssc.2022.123477>.

Supporting Information

Full details of the DFT computations and mapping of the energies onto the diagonal elements of the Heisenberg Hamiltonian.

References

- [1] K.I. Kobayashi, T. Kimura, Y. Tomioka, H. Sawada, K. Terakura, Y. Tokura, Intergrain tunneling magnetoresistance in polycrystals of the ordered double perovskite Sr₂FeReO₆, Phys. Rev. B 59 (17) (1999) 11159–11162.
- [2] J.B. Goodenough, Magnetism and the Chemical Bond, Wiley, New York, 1963.
- [3] G. Cao, L. DeLong, Frontiers of 4d- and 5d- Transition Metal Oxides, 2013, pp. 1–319.
- [4] R. Schaffer, E.K.H. Lee, B.J. Yang, Y.B. Kim, Recent progress on correlated electron systems with strong spin-orbit coupling, Rep. Prog. Phys. 79 (9) (2016), 094504.
- [5] S. Vasala, M. Karppinen, A₂B'B''O₆ perovskites: a review, Prog. Solid State Chem. 43 (1–2) (2015) 1–36.
- [6] H. Kato, T. Okuda, Y. Okimoto, Y. Tomioka, Y. Takenoya, A. Ohkubo, M. Kawasaki, Y. Tokura, Metallic ordered double-perovskite Sr₂CrReO₆ with maximal Curie temperature of 635 K, Appl. Phys. Lett. 81 (2) (2002) 328–330.
- [7] R. Morrow, R. Mishra, O.D. Restrepo, M.R. Ball, W. Windl, S. Wurmehl, U. Stockert, B. Buchner, P.M. Woodward, Independent ordering of two interpenetrating magnetic sublattices in the double perovskite Sr₂CoOsO₆, J. Am. Chem. Soc. 135 (50) (2013) 18824–18830.
- [8] P.D. Battle, G.R. Blake, T.C. Gibb, J.F. Vente, Structural chemistry and electronic properties of Sr₂FelrO₆, J. Solid State Chem. 145 (2) (1999) 541–548.
- [9] J.E. Page, C.V. Topping, A. Scrimshire, P.A. Bingham, S.J. Blundell, M.A. Hayward, Doped Sr₂FelrO₆—phase separation and a $J_{\text{eff}} \neq 0$ state for Ir³⁺, Inorg. Chem. 57 (2018), 10303.
- [10] D. Mikhailova, N. Narayanan, W. Gruner, A. Voss, A. Senyshyn, D.M. Trots, H. Fuess, H. Ehrenberg, The role of oxygen stoichiometry on phase stability, structure, and magnetic properties of Sr₂ColrO_{6-δ}, Inorg. Chem. 49 (22) (2010) 10348–10356.
- [11] S. Agrestini, K. Chen, C.Y. Kuo, L. Zhao, H.J. Lin, C.T. Chen, A. Rogalev, P. Ohresser, T.S. Chan, S.C. Weng, G. Auffermann, A. Volzke, A.C. Komarek, K. Yamaura, M.W. Haverkort, Z. Hu, L.H. Tjeng, Nature of the magnetism of iridium in the double perovskite Sr₂ColrO₆, Phys. Rev. B 100 (1) (2019), 014443.
- [12] N. Narayanan, D. Mikhailova, A. Senyshyn, D.M. Trots, R. Laskowski, P. Blaha, K. Schwarz, H. Fuess, H. Ehrenberg, Temperature and composition dependence of

- crystal structures and magnetic and electronic properties of the double perovskites $\text{La}_{2-x}\text{Sr}_x\text{CoIrO}_6$ ($0 \leq x \leq 2$), *Phys. Rev. B* 82 (2) (2010), 024403.
- [13] P.D. Battle, J.G. Gore, R.C. Hollyman, A.V. Powell, The magnetic properties of BaLaCoIrO_6 and $\text{Ba}_3\text{CoIr}_2\text{Ru}_{2-x}\text{O}_9$, *J. Alloys Compd.* 218 (1) (1995) 110–116.
- [14] K.K. Wolff, S. Agrestini, A. Tanaka, M. Jansen, L.H. Tjeng, Comparative study of potentially $J(\text{eff})=0$ ground state iridium(V) in SrLaNiIrO_6 , SrLaMgIrO_6 , and SrLaZnIrO_6 , *Z. Anorg. Allg. Chem.* 643 (23) (2017) 2095–2101.
- [15] K.K. Wolff, L.H. Tjeng, M. Jansen, The new ordered double perovskite SrLaCuIrO_6 , *Solid State Commun.* 289 (2019) 43–46.
- [16] M.P. Attfield, P.D. Battle, S.K. Bollen, T.C. Gibb, R.J. Whitehead, The crystal structure and magnetic properties of SrLaFeSnO_6 and SrLaNiSbO_6 , *J. Solid State Chem.* 100 (1) (1992) 37–48.
- [17] P. Kayser, B.J. Kennedy, B. Ranjbar, J.A. Kimpton, M. Avdeev, Spin-orbit coupling controlled ground state in the Ir(V) perovskites A_2ScIrO_6 ($\text{A} = \text{Ba}$ or Sr), *Inorg. Chem.* 56 (4) (2017) 2204–2209.
- [18] A.A. Coelho, TOPAS Academic: General Profile and Structure Analysis Software for Powder Diffraction Data, Bruker AXS, Karlsruhe, Germany, 2016.
- [19] G. Kresse, J. Furthmüller, Efficient iterative schemes for ab initio total-energy calculations using a plane-wave basis set, *Phys. Rev. B* 54 (16) (1996) 11169–11186.
- [20] G. Kresse, J. Hafner, Ab-initio molecular-dynamics for liquid-metals, *Phys. Rev. B* 47 (1) (1993) 558–561.
- [21] J.P. Perdew, K. Burke, Y. Wang, Generalized gradient approximation for the exchange-correlation hole of a many-electron system, *Phys. Rev. B* 54 (23) (1996) 16533–16539.
- [22] P.E. Blochl, Projector augmented-wave method, *Phys. Rev. B* 50 (24) (1994) 17953–17979.
- [23] S.L. Dudarev, G.A. Botton, S.Y. Savrasov, C.J. Humphreys, A.P. Sutton, Electron-energy-loss spectra and the structural stability of nickel oxide: an LSDA+U study, *Phys. Rev. B* 57 (3) (1998) 1505–1509.
- [24] J.J. Monkhorst, J.D. Pack, Special points for Brillouin zone integrations, *Phys. Rev. B* 13 (1976) 5188–5192.
- [25] D. Hobbs, G. Kresse, J. Hafner, Fully unconstrained noncollinear magnetism within the projector augmented-wave method, *Phys. Rev. B* 62 (17) (2000) 11556–11570.
- [26] V.F. Sears, Neutron scattering lengths and cross sections, *Neutron News* 3 (1992) 26–37.
- [27] I.D. Brown, D. Altermatt, Bond-valence parameters obtained from a systematic analysis of the inorganic crystal structure database, *Acta Crystallogr. B: Struct. Sci.* B41 (1985) 244–247.
- [28] N.E. Brese, M. O'Keeffe, Bond-valence parameters for solids, *Acta Crystallogr. B: Struct. Sci.* B47 (1991) 192–197.
- [29] A.V. Powell, J.G. Gore, P.D. Battle, The magnetic properties of iridium in mixed-metal oxides, *J. Alloys Compd.* 201 (1993) 73–84.
- [30] B.J. Campbell, H.T. Stokes, D.E. Tanner, D.M. Hatch, ISODISPLACE: a web-based tool for exploring structural distortions, *J. Appl. Crystallogr.* 39 (2006) 607–614.
- [31] H.T. Stokes, D.M. Hatch, B.J. Campbell, ISOTROPY Software Suite, iso.byu.edu, 2007.
- [32] G. Cao, A. Subedi, S. Calder, J.Q. Yan, J.Y. Yi, Z. Gai, L. Poudel, D.J. Singh, M.D. Lumsden, A.D. Christianson, B.C. Sales, D. Mandrus, Magnetism and electronic structure of $\text{La}_2\text{ZnIrO}_6$ and $\text{La}_2\text{MgIrO}_6$: candidate $J(\text{eff})=1/2$ Mott insulators, *Phys. Rev. B* 87 (15) (2013), 155136.
- [33] W.J. Son, P. Manuel, D. Adroja, M.H. Whangbo, Density functional analysis of the magnetic structure of Li_3RuO_4 : importance of the Ru-O . . O-Ru spin-exchange interactions and substitutional Ru defects at the Li sites, *Inorg. Chem.* 50 (19) (2011) 9400–9405.
- [34] M.H. Whangbo, H.J. Koo, D. Dai, Spin exchange interactions and magnetic structures of extended magnetic solids with localized spins: theoretical descriptions on formal, quantitative and qualitative levels, *J. Solid State Chem.* 176 (2) (2003) 417–481.
- [35] S. Kanungo, B.H. Yan, M. Jansen, C. Felser, Ab initio study of low-temperature magnetic properties of double perovskite $\text{Sr}_2\text{FeOsO}_6$, *Phys. Rev. B* 89 (21) (2014), 214414.